Ultraslow Shock Waves of Electron Density in $LiNbO_3$ Crystals

S. Gronenborn,[1] B. Sturman,[2] M. Falk,[1] D. Haertle,[1] and K. Buse[1]

[1]*Institute of Physics, University of Bonn, Wegelerstrasse 8, D-53115 Bonn, Germany*

[2]*Institute of Automation and Electrometry, Koptyug Avenue 1, 630090 Novosibirsk, Russia*

(Received 14 April 2008; published 8 September 2008)

We show, experimentally and theoretically, that the application of modest voltages, $U_0 = (0.1–1)$ kV, to $LiNbO_3$:Fe crystals at sufficiently high temperatures, $T \approx (550–700)\,^{\circ}C$, leads to the formation of ultraslow shock waves (moving discontinuities) of the electron density owing to the removal of electrons from Fe^{2+} centers. Behind the sharp wave front, almost all iron centers are in the Fe^{3+} state, the sample is optically transparent, and its transport properties are strongly modified. The front velocity decreases during the propagation; it is controlled by the electron mobility.

DOI: 10.1103/PhysRevLett.101.116601 PACS numbers: 72.20.Jv, 05.45.−a, 42.70.Nq

Solitons, periodic waves, and shock waves are the general coherent (nonrandom) structures of nonlinear physics [1–4]. Being initially a curious example of solitary waves on the surface of water, the solitons have transformed into an object which is generic for many different areas of physics, such as hydrodynamics, optics, and solid-state physics. To a somewhat smaller extent, this is applicable also to shock waves characterized by the presence of a sharp moving front (discontinuity). As is clear nowadays, this object is inherent not only in hydro- and gas dynamics, but also in such areas as acoustics and nonlinear optics [2,5]. The notion of the above coherent structures thus unifies different branches of physics; it possesses great synergy potential [3].

The concept of coherent structures is expanding in two different ways. On the one hand, researchers discover new nonlinear systems obeying the known basic equations, such as the Korteweg–de Vries equation, the nonlinear Schrödinger equation, and the Burgers equation [1,2]. On the other hand, new systems obeying essentially different model equations exhibit often similar coherent structures [4,5].

Here we report on an unambiguous and surprising shock-wave behavior in an area which has never been considered as promising for the coherent nonlinear structures. Generally, the subject is structuring of the electronic properties in solid-state materials. It is relevant to both charge-transport and optical properties, and has important applications in nonlinear optics. In contrast to many known self-organization processes, the physical background of the phenomenon found is absolutely clear.

Specifically, we are dealing with ferroelectric lithium niobate crystals ($LiNbO_3$) doped with Fe. $LiNbO_3$ is a wide-gap material which is transparent in the visible-to-near-infrared spectral range and has important applications involving the ferroelectric, electro-optic, photorefractive, and nonlinear-optic properties [6–10]. Iron is present in two charge states, Fe^{2+} and Fe^{3+}, that serve as filled and empty electron traps and determine the charge-transport properties under light [11]. The charge neutrality of $LiNbO_3$:Fe crystals is ensured by optically inactive defects, such as Li^+ and H^+ ions [12,13]. Decreasing the Fe^{2+}/Fe^{3+} ratio makes the crystals more transparent and less photorefractive sensitive in the visible. This can be achieved using different oxidization procedures.

In our experiments, congruent $LiNbO_3$ crystals doped with (0.05–2) wt % of Fe_2O_3 and a 0.025 wt % doped $LiTaO_3$:Fe crystal were used. A typical experiment was as follows: The crystal was heated slowly, $3\,^{\circ}C/\mathrm{min}$, to a designated temperature T, and then a voltage U_0 was applied to opposite faces via gold-paste electrodes. The temperatures $T = (550–700)\,^{\circ}C$ and voltages $U_0 = (0.1–1)$ kV were used. The crystallographic orientation played no role. The sample transmittance in a direction transverse to the applied field was probed each minute with a tungsten lamp and a CCD camera.

Our primary observations for a sample with 0.5 wt % doping and a Fe^{2+}/Fe^{3+} ratio of ≈ 0.2 (as-grown crystal) [14] are illustrated in Fig. 1. Initially, the sample transmittance is small owing to strong light absorption. After the voltage is applied, a fully transparent region appears

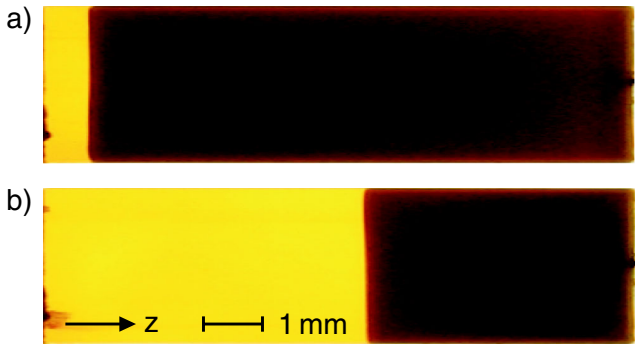

FIG. 1 (color online). Spatial distribution of transmitted light shortly after (a) the beginning and (b) in the middle of a shock-wave passage for $T = 600\,^{\circ}C$ and $U_0 = 1$ kV. For compactness, the pictures are vertically compressed by a factor of 3.

near the cathode. The border of this region moves slowly towards the anode. After a few hours the front reaches the anode, and the whole sample is fully transparent. The front width is smaller than 100 μm. The whole process looks like the propagation of an ultraslow shock wave (discontinuity) through the crystal. The shock-wave phenomenon is robust: It was observed in all investigated crystals within wide ranges of the temperatures T and the voltages U_0; see below for more detail.

To describe the shock wave, we adopt the known one-center model for Fe^{2+}/Fe^{3+} ions in $LiNbO_3$:Fe [11]: The concentration n of the free electrons in the conduction band is determined by the local balance between thermal excitation from Fe^{2+} centers (concentration $N_{Fe^{2+}}$) and recombination to Fe^{3+} traps (concentration $N_{Fe^{3+}}$). It is expected that $n \propto \exp(-\varepsilon_a/k_BT)$ with an activation energy $\varepsilon_a > 1$ eV. All introduced concentrations depend on the time t and on the coordinate z, while the total iron concentration $N_{Fe} = N_{Fe^{2+}} + N_{Fe^{3+}}$ is constant. The total concentration of the electrons, $N^- = N_{Fe^{2+}} + n$, depends on z and t because of charge transport.

Removal of a big amount of electrons, $N^- \sim 10^{19}$ cm^{-3}, from the Fe^{2+} centers would not be possible with solely electron charge transport. The presence of a strong charge compensation, i.e., a large amount of additional mobile charge carriers, is necessary. Optically inactive Li^+ ions (or Li^- vacancies) are most appropriate for this role at high temperatures [12,13,15]. Their concentration N^+ exceeds 10^{20} cm^{-3} in congruent lithium niobate.

The essence of the charge transport is expressed by the relations for the densities of ionic and electronic drift currents, j_+ and j_-:

$$j_\pm = e\mu_\pm N^\pm E, \tag{1}$$

where e is the elementary charge, $E = E(z, t)$ the electric field, μ_+ the mobility of the compensating charges, and μ_- the electron mobility related to the total electron density N^-. The right-hand side of Eq. (1) is nonlinear in E and $N^\pm$; it represents the drift nonlinearity. The diffusion components of $j_\pm$ are negligible in the leading approximation; in line with the literature [1,2], they determine the width of the shock-wave front.

With these preliminaries, we can construct the shock-wave solution. Let $N_0^\pm$ be the initial values of $N^\pm$, l the sample thickness, $U_0 > 0$ the applied voltage, and v the front velocity. This velocity depends generally on the front coordinate $z_0(t)$. In accordance with the observations, we assume that $N^- = 0$ for $0 < z < z_0$ (region 1, transparent) while $N^- = N_0^-$ for $z_0 < z < l$ (region 2, dark); see Fig. 2. Then, to meet the neutrality condition, we set $N^+ = N_0^+ - N_0^-$ for $z < z_0$ and $N^+ = N_0^+$ for $z > z_0$. Last, we denote the fields in the spatially uniform regions 1 and 2 as E_1 and E_2, respectively. All above variables experience discontinuities at $z = z_0$. The total electric current $j = j_+ + j_-$ is ionic in region 1 and electron-ionic in region 2.

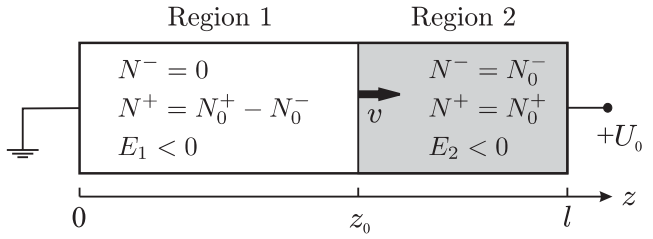

FIG. 2. Geometric scheme of the shock-wave propagation; z_0 is the front coordinate, and l is the crystal thickness.

The main requirement at the shock-wave front, which ensures continuity of the electronic current, is that the front velocity equals the electron drift velocity,

$$v = -\mu_- E_2. \tag{2}$$

Since the front is moving, the resistivities of the sequentially connected regions 1 and 2 are changing. According to the Kirchhoff laws and Fig. 2, we have $E_1 z_0 + (l - z_0)E_2 = -U_0$ and $E_1/E_2 = \sigma_2/\sigma_1 > 1$, where $\sigma_1 = e\mu_+(N_0^+ - N_0^-)$ and $\sigma_2 = e(\mu_- N_0^- + \mu_+ N_0^+)$ are the conductivities in regions 1 and 2.

The above relations give the shock-wave solution:

$$\begin{aligned} v &= \mu_- E_0/(1 + a\xi), \\ E_1/E_0 &= -(1 + a)/(1 + a\xi), \\ E_2/E_0 &= -1/(1 + a\xi), \end{aligned} \tag{3}$$

where $\xi = z_0/l$ is the normalized front coordinate, $E_0 = U_0/l > 0$ the absolute value of the average electric field, and $a = (\sigma_2 - \sigma_1)/\sigma_1 = (\mu_-/\mu_+ + 1)/(N_0^+/N_0^- - 1) > 0$. As expected, we have $E_{2,1} = -E_0$ for $\xi = 0, 1$. The coordinate dependences in Eq. (3) are controlled by the dimensionless parameter a. The front velocity $v(\xi)$ decreases during propagation from $\mu_- E_0$ to $\mu_- E_0/(1 + a)$. With increasing ratio N_0^+/N_0^-, the parameter a decreases, and the function $v(\xi)$ tends to be quasiconstant.

Since v is the time derivative of z_0, we easily obtain for the time dependence of the normalized front coordinate

$$\xi = (-1 + \sqrt{1 + 2at/t_0})/a, \tag{4}$$

where $t_0 = l/(\mu_- E_0)$ is a characteristic time. The total traveling time of the shock wave through the crystal is $t_\Sigma = t_0(1 + a/2)$.

The shock-wave propagation must be accompanied by a time-dependent electric current $j = \sigma_2 E_0/(1 + a\xi)$. According to Eq. (4), the total number of carriers flowing through a unit surface element during the shock-wave passage is $S_\Sigma = \int_0^{t_\Sigma} j(t)dt/e = lN_0^-(1 + N_0^+\mu_+/N_0^-\mu_-)$. The ratio lN_0^-/S_Σ is the fraction of electrons among the electron-ionic charge carriers escaped from the crystal; it is not controlled by the parameter a. The smaller the ratio $N_0^+\mu_+/N_0^-\mu_-$, the larger the figure of merit.

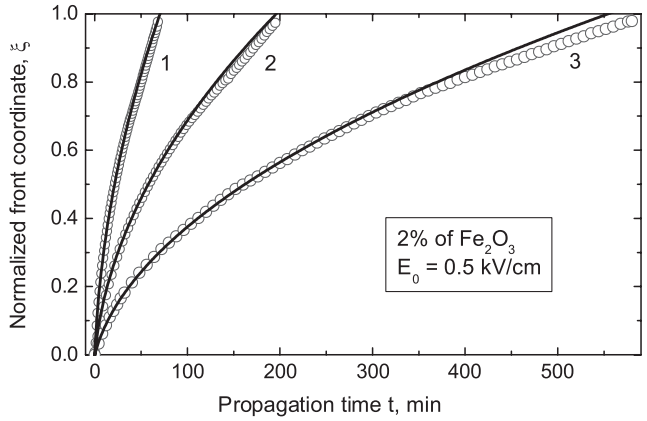

FIG. 3. The normalized front coordinate ξ versus the time for $U_0 = 0.5$ kV. The open circles for 1, 2, and 3 correspond to $T = 650$, 600, and 550 °C, respectively. The solid lines are plotted for the combinations of the model parameters ($a = 7.4$, $t_0 = 15$ min), (9.2, 35 min), and (9.8, 94 min).

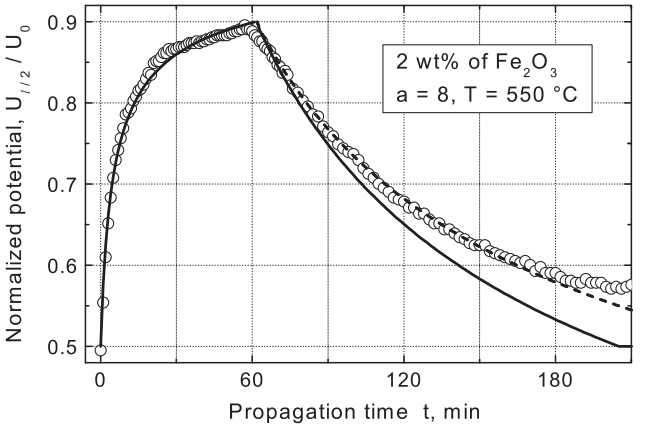

FIG. 4. Dependence $U_{l/2}(t)/U_0$. The open circles are experimental data, the solid line is plotted for $a = 8$ and $t_0 = 41$ min within the basic model, and the dashed line corresponds to a refined model (see the text). The front passes the microelectrode at $t \simeq 60$ min.

To check the model predictions and to extract further information on the charge transport, we have conducted additional experiments. First, the time dependence $z_0(t)$ was measured. The open circles in Fig. 3 are the experimental data for 2 wt % doping, $l = 1$ cm, $U_0 = 0.5$ kV, and three values of T. The solid lines are calculated from Eq. (4) using a and t_0 as fit parameters. Very good agreement between theory and experiment is evident. Small deviations occur only at the final stage, when the shock wave is approaching the anode. The wave moves here slightly slower than expected. In accordance with the model, we have a strong decrease of the front velocity $v(z_0)$ during the propagation. It is caused by the decrease of the field in the electron rich (dark) section of the crystal. The higher the temperature, the larger the mobility μ_- and velocity v. It was found additionally that both z_0 and v are proportional to the field $E_0 = U_0/l$ in the range (0.1–1) kV/cm.

Second, we have measured the electric current during the shock-wave passage. It is decreasing in accordance with the model, and the integrated current density S_Σ exceeds slightly (but persistently) the values of $N_0^- l$ measured in specially thinned samples by light absorption spectroscopy. This shows a high efficiency of the shock-wave cleaning—almost each charge carrier escaping from the crystal is an electron.

Third, using an auxiliary microelectrode (0.5 mm size) deposited at the center of the largest side face of a sample with $l = 11$ mm and a 2 wt % doping, we measured the time dependence of the voltage $U_{l/2}$ during the shock-wave passage. It is compared with the dependence $U_{l/2}(t) = -\int_0^{l/2} E(z, t)dz$, as it follows from Eqs. (3). The corresponding results for $T = 550$ °C are presented in Fig. 4 by the open circles and the solid line. Apart from a good qualitative agreement, we also have a small but remarkable discrepancy between theory and experiment at the final stage. It provides additional insight into the underlying physics and will be discussed later.

With the value of $t_0 = l/\mu_- E_0$ known, the electron mobility μ_- can be evaluated. We have thus measured the dependence $\mu_-(T)$ in the range (550–700) °C. It follows an Arrehnius law, $\mu_- \propto \exp(-\varepsilon_a/k_B T)$. Figure 5 shows a representative example of the temperature dependence for 2 wt % of Fe_2O_3. When the Fe_2O_3 content decreases from 2 to 0.5 wt %, the activation energy ε_a increases from $\simeq 1.13$ to 1.4 eV.

The sum of experimental and theoretical data shows unambiguously that application of modest electric fields, $E_0 \lesssim 1$ kV/cm, to strongly doped $LiNbO_3$:Fe crystals results within the temperature window (550–700) °C in formation of an ultraslow shock wave of the electron density, which is coupled to the discontinuity of important physical parameters such as the light-absorption coefficient and the

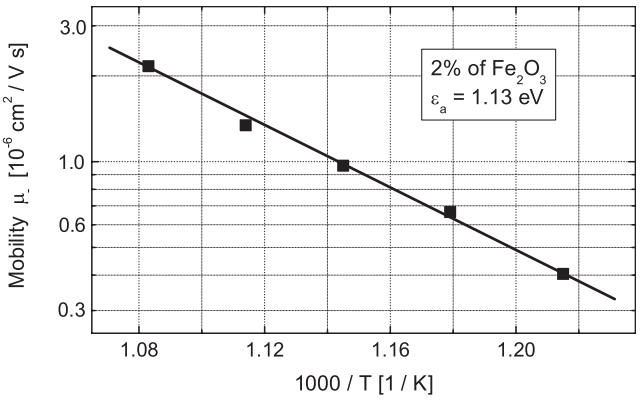

FIG. 5. Temperature dependence of the electron mobility μ_- for 2 wt % of Fe_2O_3. The solid squares represent experimental data, and the solid line is an Arrhenius fit.

electric conductivity. The shock-wave characteristics are well described within a simple model assuming uniform properties of the crystal in each of two spatial domains—before and after the front. Passing the shock wave removes the electrons trapped in the iron centers and strongly modifies the crystal properties. To the best of our knowledge, the discovered phenomenon was never observed in solid-state physics.

Consider the possible reasons for the small discrepancy between the model and experiment at the final stage: In experiment, the potential $U_{l/2}(t)$ returns not exactly to the initial value $U_0/2$; see Fig. 4. The sample thus becomes slightly nonuniform after the shock-wave passage.

One possible reason is an increasing conductivity and, therefore, a decreasing field E_2 near the anode. Using the technique of infrared absorption at 2870 nm [16,17], we have detected an increase of the concentration of H^+ ions up to $\approx 10^{19}$ cm^{-3} near the anode. Quantitatively, taking into account the spatially nonuniform H^+ contribution to the conductivity goes beyond the scope of this Letter.

Another possible reason is the growth of a low-conducting layer under the cathode. An easy detachment of this electrode after the shock-wave passage [15] supports this idea. The model can be refined using the Kirchhoff laws and assuming that the resistivity of the layer grows as the amount of lithium conveyed to the cathode. The modification is reduced to a slight renormalization of the fit parameter a in Eq. (4) and, for $\xi < 1/2$, in the expression for $U_{l/2}(\xi)$, which means virtually no changes. The dependence $U_{l/2}(\xi)$ for $\xi > 1/2$ undergoes qualitative changes. The dashed line in Fig. 4 shows the expected dependence for a 10% voltage drop in the layer after the shock-wave passage. The whole set of experimental curves in Figs. 3 and 4 becomes well fitted.

Now we consider what happens with the shock wave when changing the variable input parameters. Decreasing the temperature leads to a strong slowing down of the shock wave in agreement with the model. Increasing T above 650 °C results in deterioration of the cleaning process: The front experiences distortions, and the amount of electrons behind is increasing. Increasing the field E_0 above 1 kV/cm often leads to instabilities of the shock-wave propagation. The front becomes distorted and/or dark localized perturbations tend to appear at the cathode and propagate then towards the anode behind the front.

A decrease of the doping to 0.05 wt % results in a quasiconstant propagation velocity, $v(t)$, which is fully consistent with the model predictions. Most probably, the shock wave survives even for lower doping levels, when the light absorption is too weak to be measured. This assumption is supported by the early experiments [18] which show a considerable reduction of the Fe^{2+} related optical damage in undoped $LiNbO_3$ crystals after keeping them in an applied field at high temperatures.

In conclusion, we have shown, experimentally and theoretically, that application of modest electric fields to $LiNbO_3$:Fe crystals at sufficiently high temperatures results in the formation of ultraslow shock waves of the electron density and almost complete removal of photoexcitable electrons from the iron centers. Such a shock wave represents an entirely new phenomenon; it is important for the suppression of the optical damage in lithium niobate [10]. Being apparently simple and robust, it implies interdisciplinary issues for such areas as nonlinear dynamics, solid-state physics, and surface physics.

We thank the DFG and the Deutsche Telekom AG for financial support. Fruitful interaction with K. Brands and T. Woike is appreciated.

[1] G. B. Whitham, *Linear and Nonlinear Waves* (Wiley-Interscience, New York, 1974).
[2] A. Scott, *Nonlinear Science: Emergence and Dynamics of Coherent Structures* (Oxford University Press, New York, 2003).
[3] H. Haken, *Advanced Synergetics* (Springer-Verlag, Berlin, 1983).
[4] G. I. Stegeman and M. Segev, Science **286**, 1518 (1999).
[5] G. F. Calvo *et al.*, Phys. Rev. Lett. **89**, 033902 (2002).
[6] Yu. S. Kuzminov, *Lithium Niobate Crystals* (Cambridge International Science Publishing, Cambridge, U.K., 1999).
[7] V. S. Ilchenko *et al.*, Phys. Rev. Lett. **92**, 043903 (2004).
[8] L. E. Myers *et al.*, J. Opt. Soc. Am. B **12**, 2102 (1995).
[9] N. G. R. Broderick *et al.*, Phys. Rev. Lett. **84**, 4345 (2000).
[10] I. Breuning *et al.*, Appl. Phys. Lett. **91**, 221110 (2007).
[11] K. Buse, J. Imbrock, E. Krätzig, and K. Peithmann, *Photorefractive Effects in* $LiNbO_3$ *and* $LiTaO_3$, Photorefractive Materials and Their Applications Vol. 2, edited by P. Günter and J.-P. Huignard (Springer, New York, 2007).
[12] A. Briat *et al.*, *Defects in Inorganic Photorefractive Materials and Their Investigations*, Photorefractive Materials and Their Applications Vol. 2, edited by P. Günter and J.-P. Huignard (Springer, New York, 2007).
[13] D. P. Birnie III, J. Mater. Sci. **28**, 302 (1993).
[14] M. Falk and K. Buse, Appl. Phys. B **81**, 853 (2005).
[15] M. Falk, Th. Woike, and K. Buse, J. Appl. Phys. **102**, 063529 (2007).
[16] R. G. Smith *et al.*, J. Appl. Phys. **39**, 4600 (1968).
[17] S. Kapphan and A. Breitkopf, Phys. Status Solidi A **133**, 159 (1992).
[18] H. J. Levinstein *et al.*, J. Appl. Phys. **38**, 3101 (1967).